Supporting Information

Deng et al. 10.1073/pnas.1201052109

SI Text

Geologic Setting of Zanda Basin. Zanda Basin is a late Cenozoic basin (Fig. S1*A*) located just north of the high Himalayan ridgecrest in the west-central part of the orogen (~32° N, 80° E; elevation 3,700–4,500 m). The basin fill consists of ~800 m of fluvial, lacustrine, eolian, and alluvial fan deposits (1).

Since the initial establishment of the Zanda Formation as a lithological unit (2), additional formation (such as the Tuolin and Xiangze formations) or even group names (Zanda Group) were proposed (3), often based on a perceived depositional hiatus that later proved to be false (1, 4). Here we use a single unit name, Zanda Formation, for the entire basin sequence.

The fossils were collected from the eastern bank of the main wash of Daba Canyon in the Zanda Basin (ZD0918. GPS: 31°25′ 27.9″N, 79°45′31.1″ E; elevation: 3,937 m above sea level) (Fig. S1*A*) in a grayish-green and brownish-yellow lacustrine sandstone of the lower part of the Zanda Formation (Fig. S1*B*). A skeleton [Institute of Vertebrate Paleontology and Paleoanthropology (IVPP) V 18189] of a single individual of *Hipparion zandaense* with only the limbs, broken pelvis, and lumbar, sacral, and some caudal vertebrae in situ was collected in an area of 1.5 m × 1 m (Fig. S1*B*). The skull, vertebrae, and ribs had weathered out and were found as fragments down slope. The crano-caudal trend of the *Hipparion* skeleton is northeast-southwest. No other associated mammalian fossils were found at this locality.

Magnetochronology and Biochronology. There have been no fewer than four independent attempts at paleomagnetic age determination of the Zanda strata during the past 12 y, although only three of these provided enough documentation to be evaluated here (1, 4, 5). All three studies measured an 800+ m section for the total thickness of Zanda sediments, and arrived at roughly similar magnetic reversal patterns. On the other hand, none of the fossils in these paleomagnetic sections are well preserved or well studied enough to offer real constraints within their proposed age range of late Miocene through Pliocene.

Our own mammalian faunas are unique in offering the most restrictive age constraints so far known (6). Critically, in the lower part of the sequence, we have recovered a small mammal assemblage (IVPP localities ZD0609 and 0904) that falls in the 174- to 186-m level of the south Zanda section (1) within the top part of an alternating greenish sandstone and silt unit and just below the fine-grained lacustrine mudstone with fine laminations. The most age-diagnostic element of this small mammal assemblage is *Mimomys*, which is most comparable in level of crown heights to *Mimomys* (*Aratomys*) *bilikeensis* from the Early Pliocene Bilike locality of Inner Mongolia, which is the earliest representative of arvicoline rodents in China (7). The appearance of these rodents thus is a highly age-diagnostic event throughout northern continents. IVPP localities ZD0609 and 0904 fall in a relatively long normal chron that we interpret to be C3n.4n (i.e., 4.997–5.235 Ma in ATNTS2004) (8) (Fig. S1*C*).

Large carnivorans, such as *Chasmaporthetes* (IVPP locality ZD0908), *Vulpes* (IVPP locality ZD1001), *Nyctereutes* (IVPP locality ZD0624), and *Meles* (IVPP locality ZD1001), offer additional chronologic constraints, even though most of these are stratigraphically 30 m to more than 200 m higher than the *Mimomys* horizon. The Asiatic first occurrences of these genera are mostly confined to the Pliocene, although occasional Late Miocene records have been suggested elsewhere (9–12). Collectively, they have a distinctly Pliocene characteristic.

Overall, the fossiliferous middle Zanda sequence yields characteristic Pliocene faunas (Table S1), although the upper alluvial conglomerates and lower fluvial sandstones, from which few vertebrate fossils are found thus far, range into the Pleistocene and Miocene, respectively. Based on our paleontologic constraints, we reinterpreted previously published paleomagnetic columns from various parts of the basin, and our new age estimates (Fig. S1*C*) of the Zanda section spans ~400 ka to 6.1 Ma in GPTS of ATNTS2004 (8). Our alternative interpretation is closest (but not identical) to those proposed by Qian (5) and takes into account the fast deposition in the upper conglomerates and lower fluvial sandstones.

ZD0918 is approximately at 267 m level of leg 6 in the South Zanda section (1), and it falls near the lower end of a magnetically normal interval correlated to Chron C3n.2n (4.493–4.631 Ma, ATNTS2004). Our correlation yields an age of 4.6 Ma for ZD0918.

Description and Comparison of the Limb Bones of *Hipparion zandaense* (Figs. S2–S5; Tables S2 and S3). The postcranial bones of *H. zandaense* are close to those of *Hipparion houfenense* within the same subgenus, *Plesiohipparion* in morphology, but smaller than the latter in size (Fig. 3, Figs. S2–S5, and Tables S2 and S3) (13–18). *H. houfenense* is a typical representative in the North China Plain during the Pliocene. The forelimb of a mammal consists of the humerus, radius and ulna, carpals, metacarpals, and phalanges, and the hindlimb consists of the femur, tibia and fibula, tarsals, metatarsals, and phalanges. The representative characters of the main elements of the fore- and hindlimbs of *H. zandaense* (IVPP V 18189) are described in the following sections.

Humerus. A groove is indistinct below the characteristic lateral epicondyle crest in *Hipparion*, which is oblique postero-inferiorly. The lower part of the lateral epicondyle (i.e., the part behind the trochlea and the lateral ligament fossa) forms a narrow concave surface, the posterior margin of which forms a distinct concave line. The latero-superior side of the coronoid fossa is surrounded by a very prominent crest that is nearly parallel to the upper margin of the trochlear articulate surface and makes this part of the coronoid fossa relatively narrow (Fig. S2, 1d). The above characters are identical with those of *H. houfenense* (15). The difference between the two species is that the lateral epicondyle crest of *H. zandaense* is enlarged downward and forms a scar, the margin of which is surrounded by interrupted ridges. Measurements: minimal breadth, 28.6 mm; diameter perpendicular to, and at the level of the minimal breadth, ~36 mm; maximal depth at the level of the median tubercule, 68.4 mm; distal maximal depth, 73.7 mm; maximal trochlear height, 46.7 mm; minimal trochlear height, 33.8mm; trochlear height at the sagittal crest, 40.4 mm.

Radius. On the proximal articular surface, the lateral diameter is much smaller than the medial one, and the synovial fossa at the posterior part of the sagittal ridge is relatively large (Fig. S2, 2e). The radial tuberosity on the proximal anterior surface is weak, lateral to which there is not a distinct concave surface (Fig. S2, 2a); the proximal medial tuberosity does not exceed the medial margin of the elbow articular surface; the upper margin of the medial rough surface for ligament attachment is much lower than the round opening of the radius-ulna interosseous space (Fig. S2, 2c); the posterior margin of the proximal articular surface is straight, the latero-posterior corner of which lacks a clear sharp prominent angle posteriorly (Fig. S2, 2e); on the distal anterior surface there are two distinct ridges and three grooves, among them the lateral ridge is located at the boundary between the distal facets for the

scaphoid and lunate (Fig. S2, 2a). These characters are the same as those of *H. houfenense*. Measurements: maximal length, 281.2 mm; medial length, 272.2 mm; minimal breadth, 36 mm; depth of diaphysis at level of the minimal breadth, 23.5 mm; proximal articular breadth, 64.8 mm; proximal articular depth, 33.8 mm; proximal maximal breadth, 68 mm; distal articular breadth, 53.1 mm; distal articular depth, 31 mm; distal maximal breadth, 63 mm; breadth of the radial condyle, 22.4 mm; breadth of the ulnar condyle, 13.6 mm.

Ulna. The medial end of the proximal facet for the radius distinctly exceeds the posterior end of the sagittal ridge, and the ulna shaft does not reach the lateral side of the radius shaft; the proximal lateral tuberosity is well-developed, and exceeds the lateral border of the elbow articular surface (Fig. S2, 2b); the medial ridge-like rough surface is weak, which is located on the lower one-third of the volar surface and attaches the superficial digital flexor muscle (Fig. S2, 2c). These characters are different from those of *H. houfenense*, in which the ulna is placed more laterally relative to the radius; the medial end of the facet for the radius slightly exceeds the posterior end of the sagittal crest; the shaft exceeds the lateral side of the radius shaft so that the radius looks more robust; the proximal lateral tuberosity is weak; the ridge-like rough surface on the volar surface attached by the superficial digital flexor muscle is better developed, lateral to which is a groove, and then a ridge that separates from the medial surface of the radius. Measurements: maximal length, 349.5 mm; length of the olecranon, 68.6 mm; maximal articular breadth, 39.9 mm; minimal depth of the olecranon, 43.5 mm; depth across the processus anconaeus, 59.5 mm.

Third metacarpal. On the proximal surface, the facet for the magnum has a highly rising sharp angle on its postero-medial corner, the posterior margin of which is approximately parallel to the volar surface of the shaft; the angle between facets for the unciform and the magnum on the proximal anterior margin is large, nearly 160°, identical with that of *H. houfenense*. The whole proximal articular surface is a sector in shape, but its posterior end is not constricted to a point, and its anterior and posterior parts face in approximately the same direction (Fig. S3, 1e). Above the lateral ligament fossa, the distal rough surface for the long ligament attachment is located anteriorly, at which the contact facets for the side phalanxes have a distinct bending (Fig. S3, 1d). On the distal anterior side, there is a smooth surface with a clear border above the articular surface, but the antero-superior end of the sagittal keel does not become low (Fig. S3, 1a). Measurements are in Table S2.

Fore first phalanx III. The fore first phalanx III is very similar to that of *H. houfenense*, proportionally slender and flattened, and constricted in middle (Fig. S3, 2a and 2b). The proximal articular surface is wider than thick. The proximal rough surface extends posteriorly to a small degree (Fig. S3, 2e). The side depressions for ligamentous attachment are low, and the impressions for the attachment of the superficial digital flexor muscle are large (Fig. S3, 2c and 2d). Differently in *H. zandaense*, the proximal sagittal groove is deeper, which makes the central depression on the anterior margin more distinct (Fig. S3, 2a); the distal articular surface is more undulate (Fig. S3, 2f); the volar V-scar is rough and wide, at the basal center of which is a marked bulge. The bottom of the V-scar is rounded and extends to reach the middle level of the bone (Fig. S3, 2b). Measurements: maximal length, 67 mm; anterior length, 61.8 mm; minimal breadth, 27 mm; proximal breadth, 40.8 mm; proximal depth, 30.5 mm; distal breadth at the tuberosities, 34.4 mm; distal articular breadth, 34.8 mm; distal articular depth, 21 mm; minimal length of the V-scar, 26.8 mm; medial supratuberosital length, 53 mm; lateral supratuberosital length, 55.3 mm; medial infratuberosital length, 10.8 mm; lateral infratuberosital length, 10.9 mm.

Fore second phalanx III. The common character with *H. houfenense* is a weak sagittal ridge of the proximal articular surface (Fig. S3, 3e), and the different character is a relatively large distal and medial impression for ligamentous attachment in *H. zandaense* (Fig. S3, 3c and 3d). Measurements: maximal length, 41 mm; anterior length, 32.7 mm; minimal breadth, 34.6 mm; proximal maximal breadth, 42.1 mm; proximal maximal depth, 25.9 mm; distal articular maximal breadth, 41.6 mm.

Fore third phalanx III. The dorsal slope is a low angle (34°) (Fig. S3, 4c and 4d), compared with a 45–50° angle in the extant *Equus*. The anterior margin has a central groove. The palmar process is weak, and the dorsal groove is faint (Fig. S3, 4e and 4f). The flexor surface of the volar surface is large and distinctly prominent (Fig. S3, 4f). The grooves for attachment of the collateral ligaments are deep (Fig. S3, 4c and 4d). The proximal articular surface is trapezoidal (Fig. S3, 4b). Measurements: length from the posterior edge of the articular surface to the tip of the phalanx, 57 mm; anterior length, 57.4 mm; maximal breadth, 69.7 mm; articular breadth, 42.7 mm; articular depth, 21.9 mm; maximal height, 43.2 mm; angle between the sole and the dorsal line, 34°; circumference of the sole, 180 mm.

Comparatively, the side toes (digits II and IV) of *H. zandaense* are too short to touch the ground during movement, so they cannot assist in distributing the animal's body weight and have completely lost locomotive function, which is related to faster running speeds.

Femur. The medial epicondyle is a strongly prominent ridge. There is not a clear ridge above the medial ridge of the distal trochlea, which is wide, and the proximal rough line for the medial vastus muscle is well-developed (Fig. S4, 1c). The transition from the trochlea to the intercondyloid fossa is very steep (Fig. S4, 1f). These characters are similar to those of *Equus* but different from most species of *Hipparion*. In *Hipparion primigenium* and *Hipparion sinense*, for example, the medial epicondyle has no a ridge, and the ridge above the medial ridge is clear (15, 18). The minor trochanter is well developed, with a wide and thick rough surface, and without a sharp ridge to connect to the femoral head (Fig. S4, 1a–1c). The position of the distal supracondyloid fossa is very low, the upper border of which is only 63.5 mm from the upper margin of the condyle (Fig. S4, 1b and 1d). The shaft inferior to the anterior part of the major trochanter is straight (Fig. S4, 1a). The connecting line between the medial condyle and the trochlea is low and flat (Fig. S4, 1c). The posterior part of the major trochanter is rotated medially (Fig. S4, 1b). The distal extensor fossa is a large and deep triangle (Fig. S4, 1d). These characters are much different from those of *Equus*, but identical with those of *H. houfenense* (15). The medial and lateral trochlear ridges are divergent craniodorsally, and the former has a sharp hook on its antero-dorsal aspect (Fig. S4, 1a), which are similar to those of *Equus*. The unique character of *H. zandaense* is a sharp and prominent upper end of the medial ridge of the distal trochlea, which is much higher than the bony surface (Fig. S4, 1a). Measurements: maximal length, 346.5 mm; length from caput femoris to lateral condyle, 320.3 mm; minimal breadth, 30.6 mm; diameter perpendicular to, and at the level of the minimal breadth, 42.4 mm; proximal maximal breadth, 101.1 mm; proximal maximal depth, 66.7 mm; distal maximal breadth, 80.5 mm; distal maximal depth, 104.3 mm; maximal breadth of the trochlea, 52.3 mm; maximal depth of caput femoris, 47.3 mm.

Tibia. The tibia of *H. zandaense* is smaller than most specimens of *H. houfenense*, but identical with those of small individuals of the latter in size (15). Tibiae of the two species are very similar to each other in morphology, such as the lower part of the tibia crest produces a medial slant due to the attached area of the semitendinosus tendon (Fig. S4, 2a); the medial and lateral tubercles are widely separated from each other, with a distance of 14 mm (Fig. S4, 2b and 2e). The anterior depression for the cruciate ligamentous attachment is slightly larger than the posterior one, and both of them are shallow. The medial end of the ridge that separates the two depressions connects to the posterior end of the medial spine, and the lateral end connects to the middle part of the lateral spine (Fig. S4, 2e). The differences

between the two species include: the upper half of the proximal groove for the middle patellar ligament is rough and the lower half is smooth in *H. zandaense* (Fig. S4, 2a), whereas the rough surface for ligamentous attachment is indistinct in *H. houfenense*; the muscular sulcus is deep in *H. zandaense* (Fig. S4, 2e), but shallow in *H. houfenense* (15). The tuberosity for the posterior cruciate ligamentous attachment medial to the popliteal notch is lowly prominent (Fig. S4, 2e). Lateral to the distal lateral condyle, the lateral extensor tendon groove is deep and narrow, and the tuberosity behind the condyle is strong (Fig. S4, 2d). There is a wide and shallow medial flexor tendon groove on the posterior one-third of the medial surface of the medial condyle (Fig. S4, 2c). These two characters are similar to those of *H. houfenense*. The distal articular surface extends to an enlarged area to the medial condyle in *H. zandaense* (Fig. S4, 2f), which differs in *H. houfenense*. Measurements: maximal length, 333 mm; medial length, 323.4 mm; minimal breadth, 34.2 mm; minimal depth of the diaphysis, 33 mm; proximal maximal breadth, 87.2 mm; proximal maximal depth, 79.1 mm; distal maximal breadth, 62 mm; distal maximal depth, 41.3 mm; length of the fossa digitalis, 47.6 mm.

Astragalus. The trochlea is unsymmetrical, with a wider lateral ridge than the medial ridge; the lateral wall of the medial ridge is nearly vertical, and the medial wall has a wide wing-like surface that extends downward to reach above the distal deep fossa; the distal end of the medial ridge is weak, curved medially; the medial wall of the lateral ridge is moderately oblique, and the distal end is 10 mm apart from the distal articular surface (Fig. S5, 1a); the upper margin of the trochlear surface extends the most posteriorly at the central groove (Fig. S5, 1e). The distal articular surface is comparatively thick, with a transverse nonarticular impression on the central part of the lateral half and a rounded posterior angle (Fig. S5, 1f). These characters are identical with those of *H. houfenense*. The four facets for the calcaneum on the plantar surface (Fig. S5, 1b) are similar to those of *H. houfenense* in morphology. Both proximal and distal tuberosities on the medial surface are strong (Fig. S5, 1c), which are different from *H. houfenense* whose distal tuberosity is strong but proximal one weak (15). Measurements: maximal length, 53 mm; maximal diameter of the medial condyle, 54 mm; breadth of the trochlea, 25 mm; maximal breadth, 52 mm; distal articular breadth, 42.2 mm; distal articular depth, 33.5 mm; maximal medial depth, 44.3 mm.

Calcaneum. The calcaneum is elongated as a whole. The facets for the astragalus are corresponding to those on the planter surface of the astragalus in shape (Fig. S5, 2a and 2f). The lower part of the dorsal margin of the anterior process is oblique posteriorly, with a right angle to the distal articular surface in lateral view (Fig. S5, 2d). The plantar border of the bone is robust, but constricted in middle. The tarsal groove postero-superior to the sustentaculum tali is shallow (Fig. S5, 2b). The cochlear process is small (Fig. S5, 2c and 2d). The dorsal part of the medial surface of the sustentaculum tali lacks a clear vertical groove, which is similar to *H. houfenense*, but the medial surface is widely and shallowly concave in *H. zandaense* (Fig. S5, 2c), but flat in *H. houfenense*. The distal articular surface is narrowly mushroom-like and obviously constricted at middle in *H. zandaense* (Fig. S5, 2f), but straightly strip-like in *H. houfenense* (15). Measurements: maximal length, 103 mm; length of the proximal part, 62 mm; minimal breadth, 18.6 mm; proximal maximal breadth, 31 mm; proximal maximal depth, 46 mm; distal maximal breadth, 47 mm; distal maximal depth, 46.2 mm.

Third metatarsal. The medial facet for the first and second cuneiforms and the lateral facet for the cuboid have angles of 160° and 170°, respectively, to the middle facet for the third cuneiform at the proximal anterior margin, and two ridges separating the three facets are high (Fig. S5, 3e). On the plantar surface of the shaft, the side rough surfaces become close to each other at the upper half of the shaft, between which the concave surface does not extend to the lower one-third of the shaft. The lower end of the lateral rough surface ends at the position where the artery groove turns medially (Fig. S5, 3b). These characters are similar to those of *H. houfenense*. The plantar margin of the facet for the third cuneiforms projects posteriorly as a circular arc, obviously separating from the small lateral facet for the metatarsal IV, the direction of the latter is nearly vertical (Fig. S5, 3e). The sagittal keel of the distal trochlea is distinctly prominent at the upper margin of the dorsal surface, above which is a large and deep depression (Fig. S5, 3a). These characters are different from those of *H. houfenense*. In *H. houfenense*, the plantar margin of the facet for the third cuneiform is flat, tightly connecting the facet for the metatarsal IV, the latter faces latero-superiorly; the sagittal keel markedly becomes low at the upper margin of the dorsal surface, above which is a faint depression (15). Measurements are in Table S3.

Log ratio diagrams (Fig. 3) clearly show the differences in morphology and size between different horse species. The sagittal keel on the distal extremities of the metapodial is weak in *H. primigenium*. As a result, the lateral movement of the metapodial has not been completely diminished, and the lateral mobility is beneficial on uneven ground, such as a forested environment with trees (19). The metapodial of *H. primigenium* are more robust and shorter than those of *H. zandaense* (Fig. 3: comparative relationship between measurements 1 and 3, and Tables S2 and S3), and the distal elements of limb bones in the former is comparatively shorter than those in the latter (Fig. 4).

Hind first phalanx III. Most characters are similar to those of the fore first phalanx III, but its differences include: it is more robust and shorter (Fig. S5, 4a and 4b); the proximal medial tuberosity for ligament attachment is well developed (Fig. S5, 4e); the plantar rough V-scar lacks a basilar tubercle, but there is a marked tubercle on each side of its lower end (Fig. S5, 4b). Measurements: maximal length, 62.8 mm; anterior length, 59 mm; minimal breadth, 28 mm; proximal breadth, 41.2 mm; proximal depth, 33 mm; distal breadth at the tuberosities, 34 mm; distal articular breadth, 33 mm; distal articular depth, 21.1 mm; minimal length of the V-scar, 24 mm; medial supratuberosital length, 49.2 mm; lateral supratuberosital length, 48.4 mm; medial infratuberosital length, 13.6 mm; lateral infratuberosital length, 12.7 mm.

Hind second phalanx III. The distal width is smaller than the proximal width, so that the whole shape is a superiorly wide and inferiorly narrow trapezoid (Fig. S5, 5a and 5b). The distal ligament fossae face laterally and medially, respectively, and they are nearly rounded (Fig. S5, 5c and 5d). The sagittal ridge of the proximal articular surface is weak (Fig. S5, 5e), which is similar to *H. houfenense* (15). Measurements: maximal length, 40.4 mm; anterior length, 30.4 mm; minimal breadth, 33.9 mm; proximal maximal breadth, 42.1 mm; proximal maximal depth, 25.9 mm; distal articular maximal breadth, 36.7 mm.

Based on a reconstruction of the Zanda skeleton limb bones, *H. zandaense* is a large three-toed horse with a shoulder height of 1.45 m in life. This reconstructed body size is similar to the extant Przewalsky's horse (*Equus przewalskii*, 1.26–1.48 m) and the Tibetan wild ass (*Equus kiang*, 1.53–1.59 m), but larger than the earliest Eurasian *Hipparion* (*H. primigenium*, 1.36 m) (18).

Paleoenvironment Estimates Based on Stable Isotopes. Carbon and oxygen isotope ratios of fossil tooth enamel contain valuable information about the diet and water composition (20–23). We analyzed the carbon and oxygen isotopic compositions of 110 serial and bulk enamel samples from 25 teeth or tooth fragments from a diverse group of middle Pliocene mammals and 60 bulk and serial enamel samples from nine teeth from eight modern Tibetan wild asses (*E. kiang*) from Zanda Basin.

The $\delta^{13}C$ values of enamel samples from modern wild Tibetan asses from Zanda Basin are $-8.8 \pm 1.7‰$ ($n = 60$ enamel samples from eight individuals), which indicate a C_3-based diet and are consistent with the current dominance of C_3 vegetation in the

area. The enamel-$\delta^{13}C$ values of fossil horses, rhinos and bovids for the time period of 3.1–4.0 Ma are $-9.6 \pm 0.8‰$ ($n = 110$ enamel samples from 25 teeth), indicating that these ancient herbivores, like modern Tibetan asses, fed primarily on C_3 vegetation and lived in an environment dominated by C_3 plants (Fig. S6*A*). Enamel samples from the mid-Pliocene large herbivores yielded $\delta^{18}O$ values that are generally lower than those of modern Tibetan asses (Fig. S6*B*), likely indicating a shift to more arid conditions in the basin after the mid-Pliocene.

Paleo-Altimetry Estimates Based on Locomotive Functions. Scott (24) has suggested very early in his studies of evolution that everything has been killed to speed in the horses, making the animal a "cursorial machine." The locomotive function of animals is tightly linked to their musculoskeletal systems. A clear picture of how animals move is essential to understanding many of their adaptations and life strategies (25). Our locomotive analysis and comparison of limb bones show that *H. zandaense* lived in an open alpine steppe habitat and spent a significant amount of time to graze, so it evolved to have an ability of fast running and long-time standing. The timberline is a boundary between two extremely distinct ecosystems of the closed forest and the open grassland in vegetation vertical zones, is sensitive to global and regional climate changes, and is regarded as a result of long-term climate patterns. The unique environmental conditions of temperature, heat, and moisture in alpine areas restrict tree growth, and form an upper limit for forests. Factors that determine the elevation of the timberline are numerous, including latitude, longitude, and climate, among which, temperature is the most decisive climatic factor to influence the timberline (26). The distribution of vegetation vertical zones is directly related to the atmospheric temperature, and elevation of the timberline increases as temperature ascends in the growing season (27). As a result, the open alpine steppe habitat, where *H. zandaense* lived, must indicate an exact elevational range in vertical zone classification. Because a temperature increase of 2.5 °C during the mid-Pliocene (28) would make the boundaries of the vegetation vertical zones about 400 m higher, and the present elevation of the fossil locality is close to 4,000 m, the timberline in the Zanda area, by extrapolation, would have been at a maximum elevation of 4,000 m at that time.

1. Saylor JE, et al. (2009) The late Miocene through present paleoelevation history of southwestern Tibet. *Am J Sci* 309:1–42.
2. Zhang QS, Wang FB, Ji HX, Huang WB (1981) Pliocene stratigraphy of Zhada Basin, Tibet. *J Stratigr* 5:216–220.
3. Zhu DG, et al. (2005) Redefinition and redivision of the Pliocene-early Pleistocene lacustrine strata in Zanda Basin, Ngari, Tibet, China. *Geol Bull China* 24:1111–1120.
4. Wang SF, Zhang WL, Fang XM, Dai S, Kempf O (2008) Magnetostratigraphy of the Zanda Basin in southwest Tibet Plateau and its tectonic implications. *Chin Sci Bull* 53: 1393–1400.
5. Qian F (1999) Study on magnetostratigraphy in Qinghai-Tibetan plateau in late Cenozoic. *J Geom* 5:22–34.
6. Deng T, et al. (2011) Out of Tibet: Pliocene woolly rhino suggests high-plateau origin of Ice Age megaherbivores. *Science* 333:1285–1288.
7. Qiu ZD, Storch G (2000) The early Pliocene micromammalian fauna of Bilike, Inner Mongolia, China (Mammalia: Lipotyphla, Chiroptera, Rodentia, Lagomorpha). *Senckenbergiana lethaea* 80:173–229.
8. Lourens L, Hilgren F, Shackleton NJ, Laskar J, Wilson J (2004) *The Neogene Period. A Geologic Time Scale 2004*, eds Gradstein FM, Ogg JG, Smith AG (Cambridge Univ Press, Cambridge), pp 409–440.
9. Qiu ZX (1987) The Ruscinian and Villafranchian hyaenids of China. *Münchner Geowiss Abh* 9:1–109.
10. Qiu ZX, Tedford RH (1990) A Pliocene species of *Vulpes* from Yushe, Shanxi. *Vert PalAsiat* 28:245–258.
11. Tedford RH, Qiu ZX (1991) Pliocene *Nyctereutes* (Carnivora: Canidae) from Yushe, Shanxi, with comments on Chinese fossil raccoon-dogs. *Vert PalAsiat* 29:176–189.
12. Qiu ZX, Deng T, Wang BY (2004) Early Pleistocene mammalian fauna from Longdan, Dongxiang, Gansu, China. *Palaeont Sin New Ser C* 27:1–198.
13. Zheng SH (1980) The *Hipparion* fauna of Bulong Basin, Biru, Xizang. *Palaeontology of Xizang, Book 1*, ed Chinese Academy of Sciences (Science Press, Beijing), pp 33–47.
14. Eisenmann V, Beckouche S (1986) Identification and discrimination of metapodials from Pleistocene and modern *Equus*, wild and domestic. *Equids in the Ancient World*, eds Meadow RH, Uerpmann H-P (Dr. Ludwig Reichert Verlag, Wiesbaden), pp 117–163.
15. Qiu ZX, Huang WL, Guo ZH (1987) The Chinese hipparionine fossils. *Palaeont Sin New Ser C* 25:1–243.
16. Eisenmann V, Alberdi MT, de Giuli C, Staesche U (1988) *Studying Fossil Horses, Volume I: Methodology* (E. J. Brill, Leiden).
17. Dive J, Eisenmann V (1991) Identification and discrimination of first phalanges from Pleistocene and modern *Equus*, wild and domestic. *Equids in the Ancient World*, eds Meadow RH, Uerpmann H-P (Dr. Ludwig Reichert Verlag, Wiesbaden), pp 278–333.
18. Bernor RL, Tobien H, Hayek L-AC, Mittmann H-W (1997) *Hippotherium primigenium* (Equidae, Mammalia) from the late Miocene of Höwenegg (Hegao, Germany). *Andrias* 10:1–230.
19. Eisenmann V (1995) What metapodial morphometry has to say about some Miocene *Hipparions. Paleoclimate and Evolution, with Emphasis on Human Origins*, eds Vrba ES, Denton GH, Partridge TC, Burckle LH (Yale Univ Press, New Haven), pp 148–164.
20. Cerling TE, et al. (1997) Global vegetation change through the Miocene/Pliocene boundary. *Nature* 389:153–158.
21. Kohn MJ, Law J (2006) Stable isotope chemistry of fossil bone as a new paleoclimate indicator. *Geochim Cosmochim Acta* 70:931–946.
22. Zanazzi A, Kohn MJ, MacFadden BJ, Terry DO (2007) Large temperature drop across the Eocene-Oligocene transition in central North America. *Nature* 445:639–642.
23. Wang Y, et al. (2008) Stable isotopic variations in modern herbivore tooth enamel, plants and water on the Tibetan Plateau: Implications for paleoclimate and paleoelevation reconstructions. *Palaeogeogr Palaeoclimatol Palaeoecol* 260:359–374.
24. Scott WB (1917) *The Theory of Evolution* (Macmillan, New York).
25. MacFadden BJ (1992) *Fossil Horses: Systematics, Paleobiology, and Evolution of the Family Equidae* (Cambridge Univ Press, Cambridge).
26. Tranquillni W (1979) *Physiological Ecology of the Alpine Timberline* (Springer, Berlin).
27. Wang XP, Zhang L, Fang JY (2004) Geographical differences in alpine timberline and its climatic interpretation in China. *Acta Geogr Sin* 59:871–879.
28. Dowsett HJ (2007) The PRISM paleoclimate reconstruction and Pliocene sea-surface temperature. *Micropaleont Soc Spec Pub* 2:459–480.

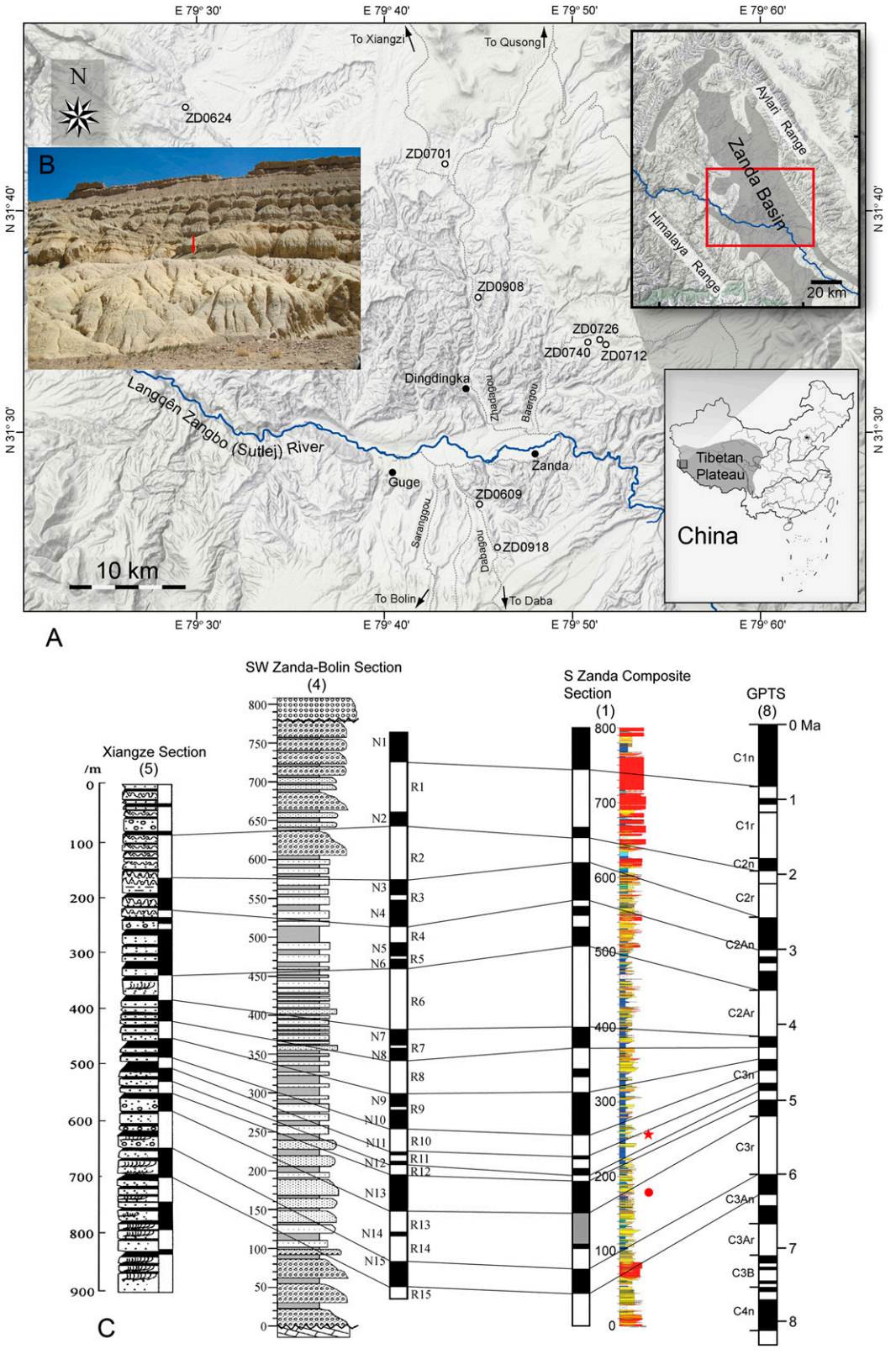

Fig. S1. (*A*) Map showing important fossil localities and important geographic locations of the Zanda Basin in Ngari, Tibet, China, including the horse skeleton locality ZD0918. (*B*) Exposures of fluvial and lacustrine sediments of the Zanda Formation, where (ZD0918) the skeleton of *H. zandaense* (IVPP V18189) was excavated. (*C*) Correlation of three published paleomagnetic sections and stratigraphic positions of key Zanda fossil mammal localities. Red star indicates *Hipparion* skeleton locality (ZD0918) and red circle indicates key fossil sites (ZD0609, 0904) for biochronologic constraints. Ages for magnetic chrons in the Geomagnetic Polarity Time Scale (GPTS) are based on ATNTS2004 (8).

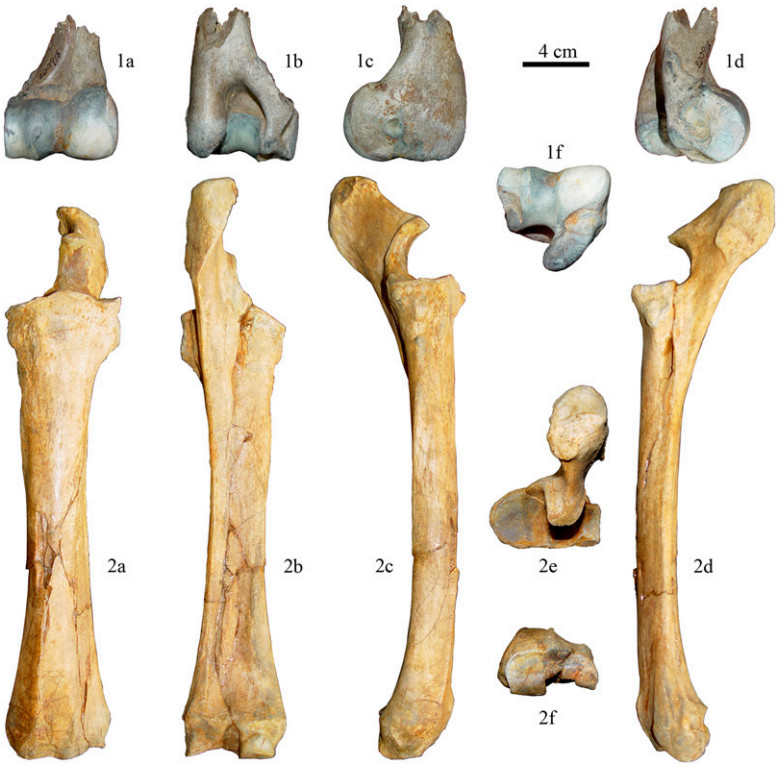

Fig. S2. Right humerus (1), and left radius and ulna (2) of *H. zandaense* from Zanda: a, anterior view; b, posterior view; c, medial view; d, lateral view; e, proximal view; f, distal view. The proximal part of the humerus is absent.

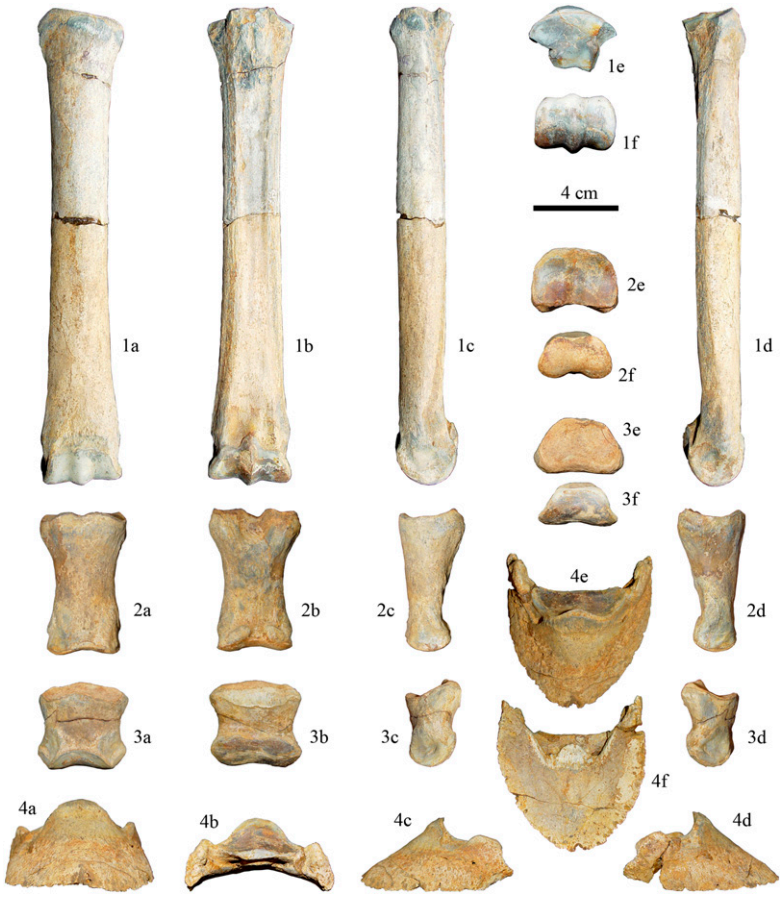

Fig. S3. Right metacarpal (Mc) III (1), and fore first (2), second (3), and third (4) Ph III of *H. zandaense* from Zanda: a, anterior view; b, posterior view; c, medial view; d, lateral view; e, proximal view; f, distal view.

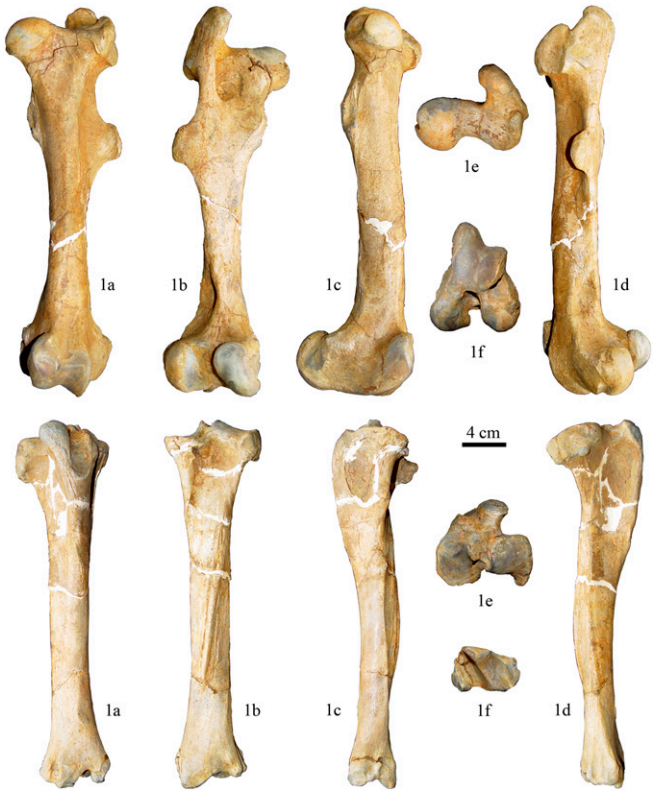

Fig. S4. Left femur (1) and right tibia (2) of *H. zandaense* from Zanda: a, anterior view; b, posterior view; c, medial view; d, lateral view; e, proximal view; f, distal view.

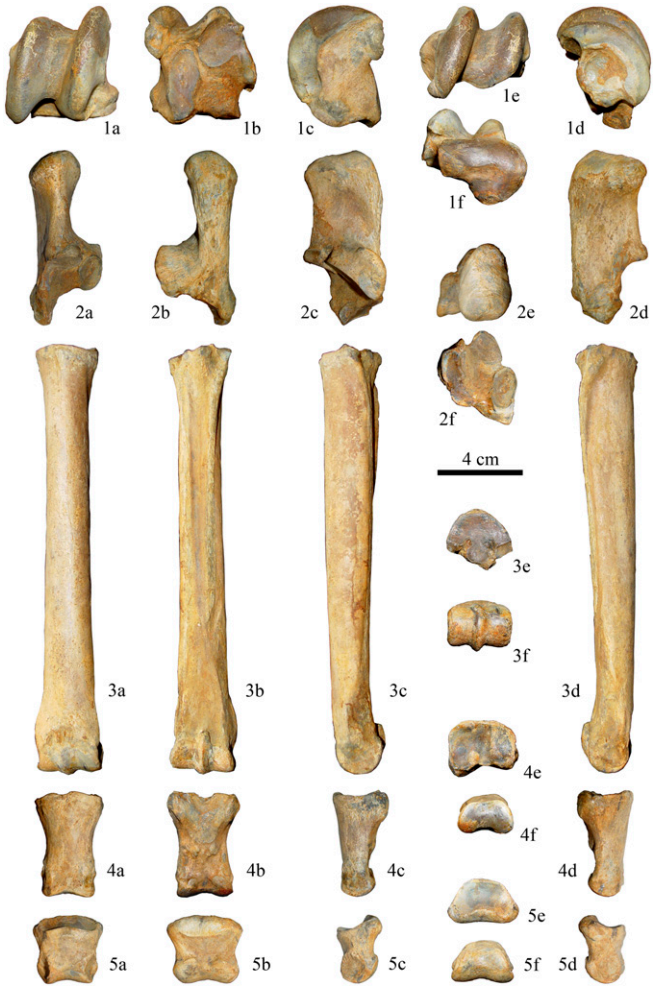

Fig. S5. Right astragalus (1), calcaneum (2), metatarpal (Mt) III (3), and hind first (4), and second (5) Ph III of *H. zandaense* from Zanda: a, anterior view; b, posterior view; c, medial view; d, lateral view; e, proximal view; f, distal view.

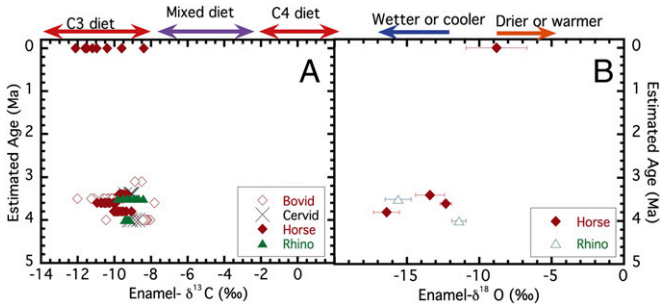

Fig. S6. (*A*) δ^{13}C values of bulk and serial enamel samples from herbivores; (*B*) the mean enamel δ^{18}O values of obligate drinkers in the Zanda Basin.

Table S1. Composite list of vertebrate taxa from the Zanda strata

Vertibrate taxa	IVPP locality number
Osteichthyes	
Cyprinidae	
Mammalia	
Insectivora	
Soricidae indet.	ZD0609, 1001
Carnivora	
Nyctereutes cf. *N. tingi*	ZD0624
Vulpes sp. nov.	ZD1001
Panthera (*Uncia*) sp. nov.	ZD1001
Meles sp. nov.	ZD1001, ZD1004
Mustela sp.	ZD1001
Chasmaporthetes sp.	ZD0908, 1029, 0636
Perissodactyla	
Hipparion zandaense	ZD0701, 0918, and others
Coelodonta thibetana	ZD0740
Artiodactyla	
Cervavitus sp. nov.	ZD0624
?*Pseudois* sp. nov.	ZD0712
Antilospira/Spirocerus sp.	ZD0701, 1001
Qurliqnoria sp.	ZD0604, 0745
Bovidae gen. A	ZD1001
Bovidae gen. B	ZD1001
Proboscidea	
Gomphotheriidae indet.	ZD0746, 1015, 1033, 1036, 1046, 1048
Rodentia	
Aepyosciurus sp.	ZD1001)
Nannocricetus sp.	ZD0609, 1001
Cricetidae gen. et sp. nov.	ZD1001
Prosiphneus cf. *P. eriksoni*	ZD1001
Mimomys (*Aratomys*) *bilikeensis*	ZD0609, 0904
Apodemus sp.	ZD0609, 0904
Lagomorpha	
Trischizolagus cf. *T. mirificus*	ZD0609, 0904
Trischizolagus cf. *T. dumitrescuae*	ZD0726, 1001
Ochotona sp. 1	ZD0609, 0904
Ochotona sp. 2	ZD0609, 0902, 0904
Ochotona sp. 3	ZD1001
Ochotona sp. 4	ZD0726

Table S2. Measurements and comparison of Mc III between *Hipparion zandaense* and other equid species

Measurement	*H. zan.* V 18189 (mm)	*H. hou.* *n* = 19–23 (mm)	*H. sin.* *n* = 15–17 (mm)	*H. pat.* *n* = 6–8 (mm)	*H. xiz.* *n* = 2 (mm)	*H. pri.* *n* = 10–16 (mm)	*H.* sp. *n* = 2 (mm)	*E. hem.* *n* = 14–16 (mm)	*E. kia.* *n* = 4 (mm)
1	225.5	249.8	274.5	234.3	213	212.8	219.5	212	242
2	217.3	—	—	—	210	207.4	213.5	206	234
3	26.3	32.8	32.9	29.1	30.5	31.7	26.3	25.9	27.8
4	22.5	27.2	29.3	24.1	23.4	22.5	23	21.1	23.4
5	41.3	49.1	50.6	43.4	~42	39.9	40.6	43.2	46.3
6	27.4	34.3	34.8	30.7	29.5	27.9	26.5	27.1	30.1
7	34.7	—	—	—	32	34.6	33.5	34.2	37.4
8	11.9	—	—	—	11.8	11.7	12.7	12.3	13.8
9	4.5	—	—	—	—	7.5	—	1.9	1.9
10	37.3	43.4	44.1	39.7	38	39.5	37.3	38.7	43.3
11	38.4	43.9	42.4	38.8	38.2	37.1	35.3	38.5	41.3
12	30	36.1	36.9	32.8	28.5	28.3	30	29.4	30.9
13	25.3	30	30.6	28.5	24.3	24.8	~25.2	~24.1	~25.8
14	27.7	~33.3	~34.1	~30.3	28	26.4	26.2	25.9	28.5
15	82	—	—	—	110.3	—	—	—	—
16	3.8	—	—	—	3.5	—	—	—	—

Abbreviations and sources: E. hem., *Equus hemionus onager* (14); and E. kia., *Equus kiang* (14); H. hou., *Hipparion houfenense* (15); H. pat., *Hipparion pater* (15); H. pri., *Hipparion primigenium* (18); H. sin., *Hipparion sinense* (15); H. xiz., *Hipparion xizangense* (13); H. zan., *Hipparion zandaense*; H. sp., *Hipparion* sp. from Khirgiz Nur, Mongolia. Measurements: 1, maximal length; 2, medial length; 3, minimal breadth; 4, depth of the diaphysis at level of 3; 5, proximal articular breadth; 6, proximal articular depth; 7, maximal diameter of the articular facet for the third carpal; 8, diameter of the anterior facet for the fourth carpal; 9, diameter of the articular facet for the second carpal; 10, distal maximal supra-articular breadth; 11, distal maximal articular breadth; 12, distal maximal depth of the keel; 13, distal minimal depth of the lateral condyle; 14, distal maximal depth of the medial condyle; 15, angle measuring the dorsal-volar development of the keel; 16, diameter of the posterior facet for the fourth carpal (16).

Table S3. Measurements and comparison of Mt III between *Hipparion zandaense* and other equid species

Measurement	*H. zan.* V 18189 (mm)	*H. hou.* *n* = 18–24 (mm)	*H. sin.* *n* = 14–18 (mm)	*H. pat.* *n* = 8–9 (mm)	*H. xiz.* *n* = 2–4 (mm)	*H. pri.* *n* = 16–24 (mm)	*E. hem.* *n* = 14–16 (mm)	*E. kia.* *n* = 4 (mm)
1	253.2	273.8	320.3	266.1	247.7	242.5	247.5	279.3
2	248.4	—	—	—	242.6	237.2	242	274.5
3	25.6	31.7	33.8	27.3	30.4	31.4	25.1	26.6
4	28	31.5	34.7	28.3	29.4	28.6	25.3	27.3
5	39	47.8	50.7	42.1	42.1	41.8	40.5	44.1
6	36	37.7	40.2	34.1	37.5	34.3	35	40.4
7	37.1	—	—	—	38.7	39.5	36	39.6
8	7.9	—	—	—	9.9	9.9	8.7	10.5
9	8.6	—	—	—	7.5	6.5	6.2	5.6
10	38.1	43.8	46.7	39.2	39.3	39.7	38.2	42.5
11	38.5	42.9	42.5	37.8	37.9	37.8	37.4	40.5
12	30	35	38.5	31.7	32.6	30.7	30.1	32.4
13	24	~28.4	~30.8	~25.1	26.1	25.3	~23.7	~26.1
14	27.2	~31.7	~34.9	~28.7	30.1	27.3	26.2	28.9
15	90	—	—	—	100	—	—	—

Abbreviations and sources: E. hem., *Equus hemionus onager* (14); and E. kia., *Equus kiang* (14); H. hou., *Hipparion houfenense* (15); H. pat., *Hipparion pater* (15); H. pri., *Hipparion primigenium* (18); H. sin., *Hipparion sinense* (15); H. xiz., *Hipparion xizangense* (13); H. zan., *Hipparion zandaense*; H. sp., *Hipparion* sp. from Khirgiz Nur, Mongolia. Measurements: 1, maximal length; 2, medial length; 3, minimal breadth; 4, depth of the diaphysis at level of 3; 5, proximal articular breadth; 6, proximal articular depth; 7, maximal dismeter of the articular facet for the third tarsal; 8, diameter of the articular facet for the fourth tarsal; 9, diameter of the articular facet for the second tarsal; 10, distal maximal supra-articular breadth; 11, distal maximal articular breadth; 12, distal maximal depth of the keel; 13, distal minimal depth of the lateral condyle; 14, distal maximal depth of the medial condyle; 15, angle measuring the dorso-volar development of the keel (16).